Nanoscale Research Letters

NANO EXPRESS Open Access

Dual-Mode On-to-Off Modulation of Plasmon-Induced Transparency and Coupling Effect in Patterned Graphene-Based Terahertz Metasurface

Zhimin Liu[1,2*], Enduo Gao[1], Zhenbin Zhang[1], Hongjian Li[3*], Hui Xu[3], Xiao Zhang[1], Xin Luo[1] and Fengqi Zhou[1*]

Abstract

The plasmon-induced transparency (PIT), which is destructive interference between the superradiation mode and the subradiation mode, is studied in patterned graphene-based terahertz metasurface composed of graphene ribbons and graphene strips. As the results of finite-difference time-domain (FDTD) simulation and coupled-mode theory (CMT) fitting, the PIT can be dynamically modulated by the dual-mode. The left (right) transmission dip is mainly tailored by the gate voltage applied to graphene ribbons (stripes), respectively, meaning a dual-mode on-to-off modulator is realized. Surprisingly, an absorbance of 50% and slow-light property of 0.7 ps are also achieved, demonstrating the proposed PIT metasurface has important applications in absorption and slow-light. In addition, coupling effects between the graphene ribbons and the graphene strips in PIT metasurface with different structural parameters also are studied in detail. Thus, the proposed structure provides a new basis for the dual-mode on-to-off multi-function modulators.

Keywords: Plasmon-induced transparency, Graphene, Dual-mode on-to-off modulation, Metasurface

Introduction

At present, surface plasmon polaritons (SPPs), as a carrier for transmitting information and energy, have become a research hotspot in the sub-wavelength optics. Generally, they are produced by the interaction between the photons in the incident light field and the electrons on the metal or insulator surface [1, 2]. The SPPs facilitate the development and manufacture of highly integrated optics and photonic circuits owing to their unique optical properties. Firstly, they are non-radiative modes with great near-field enhancement effects. Secondly, the SPPs can break through the traditional optical diffraction limitation and localize the light in the sub-wavelength range [3]. Thirdly, their properties depend on the physical parameters of the surrounding material. Therefore, SPPs-based metal-dielectric-metal (MDM) waveguides have been widely studied by scholars owing to their low-bending loss, strong local capability, and low manufacturing difficulty. At the same time, many types of MDM plasmonic waveguides have been proposed, such as splitters [4, 5], demultiplexers [6, 7], filters [8–10], and sensors [11, 12]. However, it is particularly inconvenient to obtain a specific frequency or wavelength that the MDM waveguide can only be statically modulated. Graphene, as a two-dimensional planar honeycomb structure can support the propagation of the SPPs in the mid-infrared and THz range, becomes the most promising candidate in many plasmonic materials owing to many excellent optical properties such as strong locality, low loss, near field enhancement, dynamic adjustability, etc [13, 14]. Consequently, graphene-based plasmonic optics has been used in many applications, for example, light-sensing [15, 16], absorption [17–19], switching [20], and other fascinating phenomena such as nonlinear optics [21, 22] and plasmon-induced transparency (PIT) [23–26]. The PIT effect,

* Correspondence: liuzhimin2006@163.com; lihj398@126.com; zhoufengqi2004@163.com
[1]School of Science, East China Jiaotong University, Nanchang 330013, China
[3]School of Physics and Electronics, Central South University, Changsha 410083, China
Full list of author information is available at the end of the article

which is the result of destructive interference between the superradiation mode and the subradiation mode, has produced a variety of plasmonic applications, for example, plasmonic switching [20, 27], slow-light propagation [28], holographic imaging [29], and optical storage [30]. To achieve such a complex interaction between the light and the matter, the PIT can be obtained in heterogeneous graphene ribbons [31], single-layer or multilayer graphene [32–34], and graphene-based metasurfaces [35]. However, these plasmonic devices are not only rather complicated in design, but also single-mode in terms of the modulation. Moreover, it is mainly that the resonance frequency will be tuned by manipulating the Fermi level of graphene in the modulation of most plasmonic devices. Since the transmittance of the PIT is neglected, the on-to-off modulation cannot be realized.

In this study, the proposed PIT metasurface, which consists of the periodic graphene ribbons and graphene strips, is easier to implement and fabricate. Through chemical vapor deposition (CVD) [36], the graphene ribbons and the graphene strips can be grown on the copper foil, which are transferred to a flat substrate by dry and wet transfer techniques. This technique produces fewer tears, cracks, and lower sheet resistance. Secondly, one of the most significant advantages is that the left (right) transmission dip is mainly affected by the gate voltage applied to graphene ribbons (stripes), respectively, meaning the dual-mode on-to-off modulation can be realized. Thirdly, even if the Fermi level of graphene is low, the absorption of the proposed metasurface can reach 50%, demonstrating an extraordinary absorber. Finally, when the mobility of the graphene ribbon and the graphene strip are both 3 $m^2/(Vs)$, the group delay can be as high as 0.7 ps, representing the proposed metasurface also has distinguished slow-light functions. Moreover, coupling effects between the graphene ribbons and the graphene strips in PIT metasurface with different structural parameters also are studied in detail. Therefore, this research lays a solid foundation for the dual-mode on-to-off multi-function modulator.

Methods

The configuration of the PIT metasurface composed of the patterned single-layer graphene, the electrodes, the thin metal wires, and the substrate silicon is illustrated in Fig. 1a. The graphene ribbons are connected with the left electrode to modulate their Fermi levels by the gate voltage V_{g1}. Moreover, the graphene strips are connected with the right electrode using thin metal wires, and a gate voltage V_{g2} is applied to modulate their Fermi levels [37, 38]. The gate voltages V_{g1} and V_{g2} can respectively modulate the Fermi levels of the graphene ribbons and the graphene strips to further realize the dual-mode modulation of the PIT. It is worth noting that the influence on the transmission effect can be ignored owing to the small size of the connecting wires [39]. In Fig. 1b, the Fermi level E_f of single-layer graphene can be

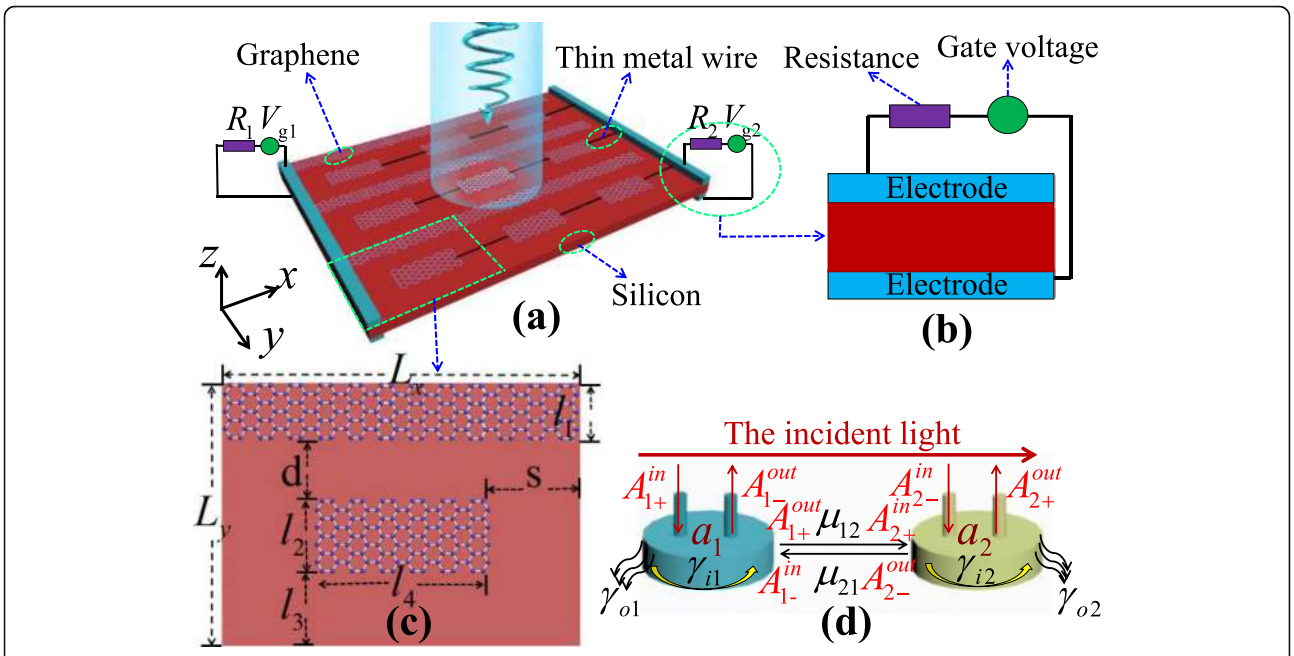

Fig. 1 **a** Schematic of the 3 × 3 unit structure of the PIT metasurface. **b** The modulated diagram of gate voltage. **c** Top view of structural unit with geometric parameters L_x = 6.0 μm, L_y = 4.0 μm, l_1 = 1.0 μm, l_2 = 1.4 μm, l_3 = d = 0.8 μm, l_4 = 2.9 μm, and S = 1.55 μm. **d** Coupling diagram between the graphene ribbon and the graphene strip

indirectly modulated by the gate voltage, which can be expressed as [40]:

$$E_f = \hbar v_F \sqrt{\frac{\pi \varepsilon_0 \varepsilon_d V_g}{e d_0}}. \tag{1}$$

Here, $\hbar$, ε_d, ε_0, e, d_0, and v_F are the reduced Planck constant, the static permittivity of silicon, the vacuum permittivity, the electron charge, the silicon thickness, and the Fermi velocity, respectively. It is worth mentioning that the carrier concentration as high as 4×10^{18} m^{-2} in graphene sheet was observed by employing an electrolytic gate, meaning E_f = 1.17 eV [41]; using this method, the Fermi energy level of graphene could be experimentally modified from 0.2 eV to 1.2 eV after applying a high bias voltage [42]. The structural unit of the proposed PIT metasurface, which consists of a graphene ribbon and a graphene strip placed on the substrate silicon, as illustrated in Fig. 1c. The periodicity is taken as L_x and L_y; the coupling distance between the graphene ribbon and the graphene strip is d; the lateral displacement of the graphene strip is S.

The optical conductivity of a single-layer graphene sheet is mainly composed of inter-band and intra-band contributions [43–45], which can be expressed as

$$\varepsilon(\omega) = 1 + \frac{\sigma_g}{\varepsilon_0 \omega \Delta} i. \tag{2}$$

$$\sigma_g = \sigma^{\text{intra}} + \sigma^{\text{inter}}. \tag{3}$$

$$\sigma^{\text{intra}} = \frac{2ie^2 k_B T}{\pi \hbar^2 (\omega + i\tau^{-1})} In\left[2 \cosh\left(\frac{E_f}{2k_B T}\right)\right]. \tag{4}$$

$$\sigma^{\text{inter}} = \frac{ie^2(\omega + i\tau^{-1})}{4\pi k_B T} \int_0^{+\infty} \frac{G(\xi)}{\hbar^2(\omega + i\tau^{-1})^2/(2k_B T)^2 - \xi^2} d\xi. \tag{5}$$

Here, $G(\xi) = \sinh(\xi)/[\cosh(E_f/k_B T) + \cosh\xi]$, where $\xi = \varepsilon/k_B T$. Moreover, ω, k_B, σ_g, σ_{inter}, and σ_{intra} are the angular frequency of incident light, the Boltzmann constant, the conductivity of single-layer graphene, the inter-band, and intra-band contributions, respectively. In this work, the room temperature is T = 300 K; the thickness of the graphene is Δ = 0.34 nm. σ_{inter} can be ignored owing to $k_B T \ll 2E_f$ in the terahertz band. Thus, σ_g can be expressed as

$$\sigma_g = \frac{ie^2 E_f}{\pi \hbar^2 (\omega + i\tau^{-1})}. \tag{6}$$

Here, the electron relaxation time can be expressed as $\tau = \mu_0 E_f/(e v_F^2)$ [40], with μ_0 = 1 $m^2/(Vs)$ being the graphene mobility. Besides, the propagation constant β of the incident light on the graphene surface can be expressed as [46]

$$\frac{\varepsilon_1}{\sqrt{\beta^2 - \varepsilon_1 k_0^2}} + \frac{\varepsilon_2}{\sqrt{\beta^2 - \varepsilon_2 k_0^2}} = -\frac{i\sigma_g}{\omega \varepsilon_0}. \tag{7}$$

Here, ε_1, ε_2, and k_0 are relative permittivity of silica and air, and the wave vector of the plane wave, respectively.

In Fig. 1d, the coupled-mode theory (CMT) [47] is used to fit the transmission and absorption spectra of FDTD numerical simulations. Elements A_1 and A_2 serve as two antennas to describe the coupling effect between the graphene ribbon and the graphene strip. When the incident light is illuminated from A and exited from B, the relation can be obtained by

$$\begin{pmatrix} \gamma_1 & -i\mu_{12} \\ -i\mu_{21} & \gamma_2 \end{pmatrix} \cdot \begin{pmatrix} a_1 \\ a_2 \end{pmatrix} = \begin{pmatrix} -\gamma_{o1}^{1/2} & 0 \\ 0 & -\gamma_{o2}^{1/2} \end{pmatrix} \cdot \begin{pmatrix} A_{1+}^{in} + A_{1-}^{in} \\ A_{2+}^{in} + A_{2-}^{in} \end{pmatrix}. \tag{8}$$

Here, $\gamma_{1(2)} = (i\omega - i\omega_{1(2)} - \gamma_{i1(2)} - \gamma_{o1(2)})$, in which the inter-loss coefficient is $\gamma_{i1(2)} = \omega_{1(2)}/(2Q_{i1(2)})$ and the extra-loss coefficient is $\gamma_{o1(2)} = \omega_{1(2)}/(2Q_{o1(2)})$. Additionally, $Q_{i1(2)} = \text{Re}(n_{\text{eff}})/\text{Im}(n_{\text{eff}})$ [29] is the inter-loss quality factor, which can be obtained by effective refractive index $n_{\text{eff}} = \beta/k_0$. The intra-loss quality factor can be obtained by $1/Q_{t1(2)} = 1/Q_{i1(2)} + 1/Q_{o1(2)}$, with $Q_{t1(2)} = f/\Delta f$ being the quality factor of the whole system (Δf is 3 dB bandwidth). Following the conservation of energy, coupling relationship between two antennas is as follows:

$$A_{2+}^{\text{in}} = A_{1+}^{\text{out}} e^{i\phi}, A_{1-}^{\text{in}} = A_{2-}^{\text{out}} e^{i\phi}, \tag{9}$$

$$A_{1+}^{\text{out}} = A_{1+}^{\text{in}} - a\gamma_{o1}^{1/2}, A_{2+}^{\text{out}} = A_{2+}^{\text{in}} - b\gamma_{o2}^{1/2}, \tag{10}$$

$$A_{1-}^{\text{out}} = A_{1-}^{\text{in}} - a\gamma_{o1}^{1/2}, A_{2-}^{\text{out}} = A_{2-}^{\text{in}} - b\gamma_{o2}^{1/2}, \tag{11}$$

$$A_{2-}^{\text{in}} = 0. \tag{12}$$

Here, the subscripts "+" and "–" represent that the antennas are illuminated in the same and opposite directions; the superscripts "in" and "out" represent the sign of the incident light entering and exiting the antennas. In addition, μ_{nm} (n = 1, 2, m = 1, 2, $n \neq m$) and ϕ are the coupling coefficients and the phase difference between two antennas, respectively. Thus, we can obtain the transmission coefficient and the reflection coefficient of the proposed PIT metasurface.

$$t = \frac{A_{2+}^{out}}{A_{1+}^{in}} = e^{i\phi} + \left[\gamma_{o1}\gamma_2 e^{i\phi} + \gamma_{o2}\gamma_1 + \left(\gamma_{o1}\gamma_{o2}\right)^{1/2}\left(\chi_1 e^{i\phi} + \chi_2\right)\right] \cdot \left(\gamma_1\gamma_2 - \chi_1\chi_2\right)^{-1}, \tag{13}$$

$$r = \frac{A_{1-}^{out}}{A_{1+}^{in}} = \left[\gamma_{o1}\gamma_1 + \gamma_{o2}\gamma_1 e^{i\phi} + \left(\gamma_{o1}\gamma_{o2}\right)^{1/2}\left(\chi_1 + \chi_2 e^{i\phi}\right)\right] \cdot \left(\gamma_1\gamma_2 - \chi_1\chi_2\right)^{-1}. \tag{14}$$

Where $\chi_{1(2)} = i\mu_{12(21)} + (\gamma_{o1(2)}\gamma_{o2(1)})^{1/2}e^{i\phi}$. Then, the transmission and absorption of the proposed PIT metasurface can be obtained by

$$T = t^2, A = 1 - t^2 - r^2. \tag{15}$$

Results and Discussion

Very recently, the graphene ribbons, as one of the most promising candidates in the graphene series owing to the fact that they are greatly easy to achieve experimentally and can support localized plasmons (mainly based on Fabry-Perot-like standing wave resonance) [48–50] and propagate plasmons [51, 52], have attracted a lot of attention in the field of nanophotonics. Here, we exploit the plasmonic coupling between the graphene ribbons and the graphene strips to demonstrate an excellent PIT effect.

So as to discuss the physical origin of the PIT effect, simulated transmission spectra of three graphene metasurfaces and electric field distributions of the entire structure and graphene strip at the resonance frequency are illustrated in Fig. 2a–c. In Fig. 2a, when the metasurfaces are shone by the x-polarized light, a subradiant mode can be excited in the graphene ribbon, which produces a red curve with a transmittance of 1. Meanwhile, a superradiant mode can be directly excited in the graphene strip, which brings about a black Lorentz curve with a transmission dip of 7.90%. As a result, the subradiant mode can be indirectly excited by the superradiant mode, forming a blue PIT curve with a transmission peak of 88.61% generated by the entire structure. In addition, electric field distributions of the entire structure and the graphene strip at the resonance frequency also can explain the physical origin of the PIT phenomenon. When only the graphene strips exist in the structural units of each pattern graphene metasurface, the electric field energy around the graphene strip is in an equilibrium state, as illustrated in Fig. 2c. In this case, only the weaker electric field is confined around the graphene strip, which produces a Lorentz curve with a lower quality factor. However, when a graphene ribbon is added to the metasurface, the electric field balance around the graphene strip is broken. At the moment, since the coupling effect between them, the electric field around the graphene strip is enhanced, and the graphene ribbon is also excited by the near field, as illustrated in Fig. 2b. Therefore, the electric field energy is localized around the graphene strip and the graphene ribbon surface, forming a PIT curve with higher quality factors.

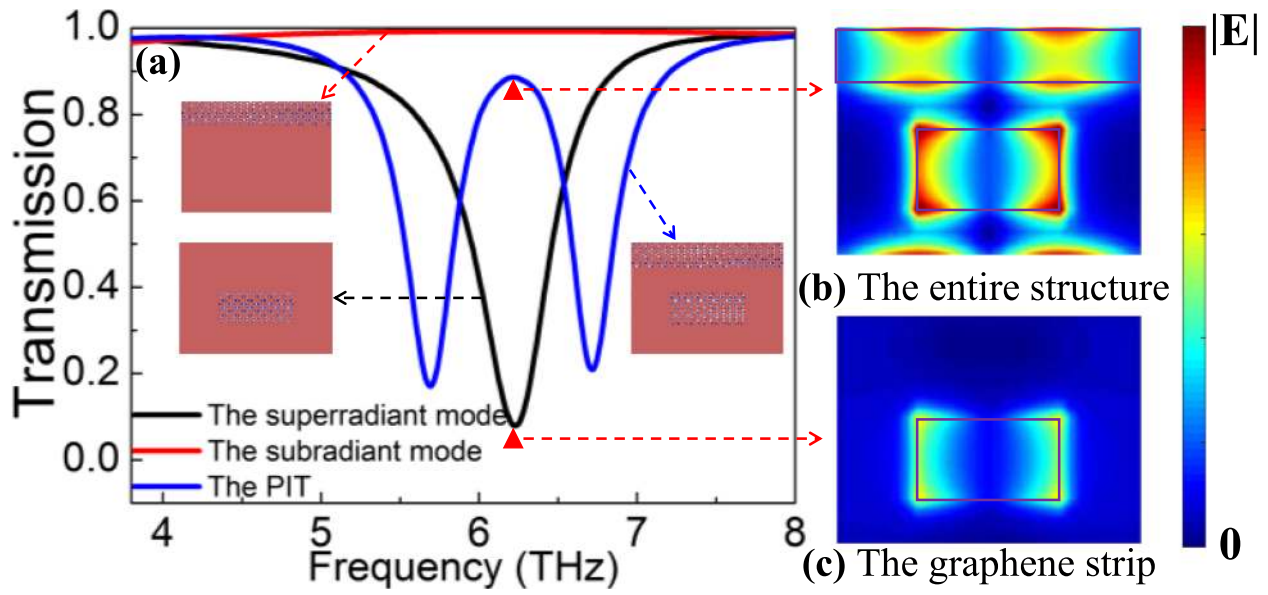

Fig. 2 **a** Simulated transmission spectra of three graphene metasurfaces. **b** Electric field distribution of the entire structure at the resonance peak. **c** Electric field distribution of the graphene strip at the resonance dip. Here, $E_{f1} = E_{f2} = 1.0$ eV

The dual-mode on-to-off modulation of PIT can be achieved by two gate voltages applied to the graphene ribbons and the graphene strips, as illustrated in Figs. 3a–h. Here, the four resonance dips are labeled "dip1, dip2, Dip1, Dip2." When the Fermi level E_{f2} of the graphene strip is fixed at 1.0 eV, the Fermi level E_{f1} of the graphene ribbon is changed to explore the PIT effect. In Fig. 3a–d, as the Fermi level E_{f1} increases from 0.6 eV to 1.2 eV, there is a significant change in dip1. For one thing, the transmittance of the dip1 is remarkably reduced indicating that an on-to-off modulation can be obtained. For another, the dip1 has an obvious blue-shift demonstrating that it is sensitive to the change of Fermi level E_{f1} and can realize frequency modulation. Besides, when the Fermi level E_{f1} of the graphene ribbon is fixed at 1.0 eV, a similar phenomenon occurs in Dip2 with the increase of the Fermi level E_{f2}. However, the blue-shift is more significantly observed in the left dip in both cases. When Fermi levels of the graphene strip and the graphene ribbon are both 1.0 eV, the resonance frequency of the superradiation mode and the monopole resonance frequency of the subradiation mode are basically 6.2 THz. Thus, the coupling between them forms a symmetrical PIT. When the Fermi level E_{f1} of the graphene ribbon is increased from 0.6 eV to 1.0 eV, the monopole resonance frequency of the subradiation mode shifted from the left side to the 6.2 THz due to the change of the graphene ribbon conductivity. In the case, the coupling between the subradiation mode and the superradiation mode is weak owing to different resonance frequencies, generating a highly asymmetric PIT. The obvious blue-shift of the dip1 in Fig. 3a–d is mainly affected by the blue-shift of the sub-radiation mode. Similarly, the obvious blue-shift of the Dip1 in Fig. 3e–h is mainly influenced by the blue-shift of the superradiation mode. The detailed on-to-off mechanism is illustrated in Fig. 3i. In the design of the on-to-off modulator, the "on" is set to a transmittance exceeding 0.3; otherwise, it is set to the "off." Thus, the proposed PIT metasurface can realize the dual-mode-on function in the Fermi level of 0.6 eV to 0.8 eV and the dual-mode-off function in the Fermi level of 0.8 eV to 1.2 eV. In short, the gate voltage V_{g1} mainly regulates the left transmission dip, yet the right transmission dip is chiefly tailored by the gate voltage V_{g2}. Therefore, a dual-mode on-to-off modulator is realized. Meanwhile, the dual-mode modulation of plasmon-induced absorption (PIA) is also obtained in Fig. 4a–h. With the increase of the Fermi level, the PIA has a clear blue-shift. Even if the Fermi level of graphene is low, the absorption of the proposed metasurface can reach 50%. This is because graphene is similar to loss properties when the Fermi level is low, resulting in high loss and absorption [53]. The phenomenon means that lower Fermi level can achieve a higher absorption, thereby reducing the required voltage. Furthermore, the transmission and absorption spectra of FDTD simulation both are fitted by CMT. Here, the blue curve indicates the FDTD simulation result; the red dotted curve indicates the CMT fitting data.

In addition, transmission spectra with different graphene mobilities are also studied, as illustrated in Fig. 5(a-c). A fully symmetrical PIT curve is obtained when $E_{f1} = E_{f2} = 1.0$ eV. On this basis, the graphene mobility is increased from 1.0 m^2/(Vs) to 3.0 m^2/(Vs) in a 1.0 m^2/(Vs) step. As the graphene mobility increases, not only the transmission spectra show apparent red-shift, but also the 3 dB bandwidth of the transmission dips becomes narrower, meaning graphene mobility can also be used to dynamically modulate the PIT and quality factors of transmission dips. Here, transmission spectra of

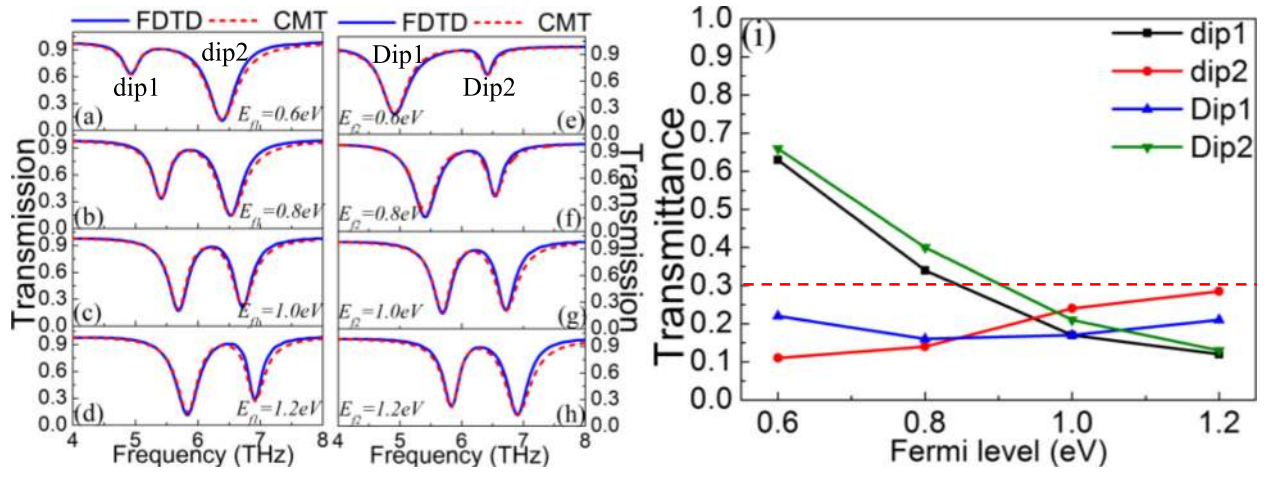

Fig. 3 Transmission spectra of FDTD simulation and CMT fitting (**a**–**d**) for different E_{f1} when E_{f2} = 1.0 eV. **e**–**h** For different E_{f2} when E_{f1} = 1.0 eV. **i** Relationship between the transmittance of resonance dip and the Fermi level

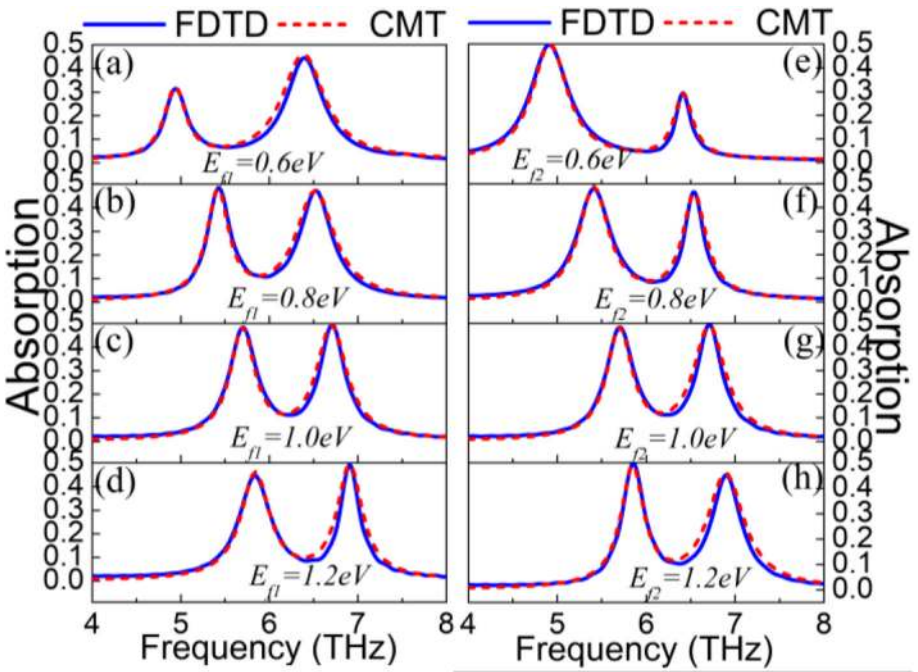

Fig. 4 Absorption spectra of FDTD simulation and CMT fitting (**a**–**d**) for different E_{f1} when E_{f2} = 1.0 eV. **e**–**h** For different E_{f2} when E_{f1} = 1.0 eV

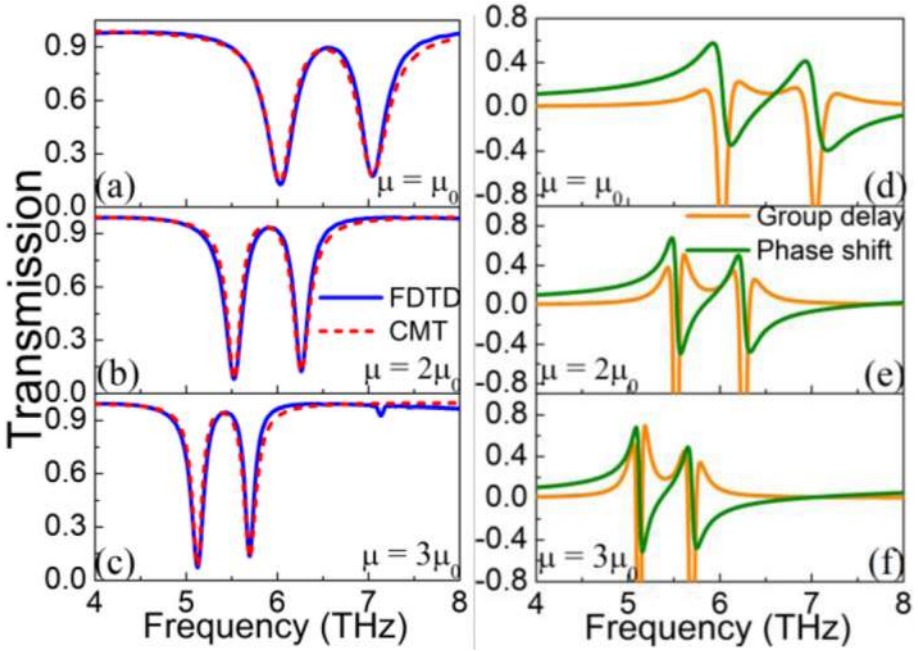

Fig. 5 a–c Transmission spectra of FDTD simulation and CMT fitting with different graphene mobility $\mu = \mu_0, 2\mu_0, 3\mu_0$. **d, e** Transmission phase shift and the group delay with different graphene mobility $\mu = \mu_0, 2\mu_0, 3\mu_0$. Here, $E_{f1} = E_{f2}$ = 1.2 eV

FDTD simulation and CMT fitting are still perfectly matched. It is known that the performances of the slow-light effect are better with the higher quality factor of the transmission dip. Therefore, the transmission phase shift and the group delay with different graphene mobilities are plotted in Fig. 5d–e. The group delay is achieved by [54]:

$$t_g = \frac{d\phi(\omega)}{d\omega}, \tag{16}$$

where $\phi(\omega)$ is the phase shift calculated by $\phi(\omega) = arg(t)$. The results show that both the group delay and the phase shift are 0 when the transmittance of the system is close to 1. Moreover, the large group delay occurs at the transmission peak and its surroundings owing to the fact that the graphene ribbon and the graphene strip have a strong coupling effect at the resonance frequency. When the graphene mobility reaches $3\mu_0$, the group delay of the system can be as high as 0.7 ps. However, the group delay at the transmission dips reaches a large negative value, meaning fast light propagation in the system. Meanwhile, the phase shift has also changed dramatically at the transmission dips. Zhang et al. recently has proposed an absorption efficiency of 50% and slow-light performance with a patterned graphene structure [25]. However, the proposed structure unit composed of graphene double strips and a graphene ribbon, which is more complex, cannot realize the dual-mode on-to-off and absorption modulation. Besides, it is unreasonable to analyze the absorption efficiency by changing the mobility of the graphene double strips with only the graphene ribbon being applied with a gate voltage. Furthermore, slow-light effect analyzed by the group index which is largely dependent on the thickness of the substrate is not objective. And the group index which can only reach 382 is poor.

Finally, coupling effects between the graphene ribbons and the graphene strips in PIT metasurface with different structural parameters are studied in detail, as illustrated in Fig. 6a–d. Other structural parameters are based on Fig. 2a. From Fig. 6a, as the coupling distance increases, the left transmission dip is first blue-shifted and then red-shifted, while the right transmission dip is basically unchanged, meaning a change of the coupling distance has a greater influence for the left transmission dip. When the lateral displacement of the graphene strip increases, the position of the transmission dips does not change owing to the x-polarized incident light, as observed in Fig. 6b. Interestingly, in Fig. 6c, the increase of l_4 results in stepped red-shift in the left transmission dip and its quality factor is getting smaller, indicating the dependence of the graphene strip length on left transmission spectra. Fig. 6d illustrates the increase of the graphene strip width causes a slight red-shift in the left transmission dip and a slight blue-shift in the right transmission dip, increasing distance between the

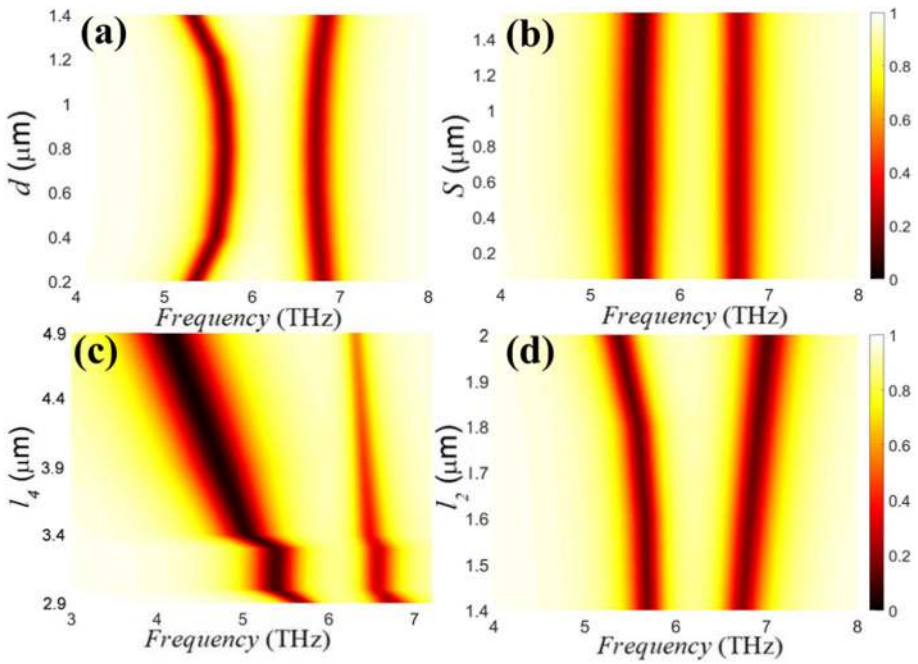

Fig. 6 Transmission spectra dependence on different geometric parameters. **a** The coupling distance, *d*, (**b**) the lateral displacement, *S*, (**c**) the length of graphene strip, l_4, (**d**) the width of graphene strip, l_2

transmission dips. It is worth mentioning that since the increments of the length and width for the graphene strip improve the inductance of the resonant system, a significant phenomenon is generated.

Conclusion

In short, we have numerically simulated and theoretically calculated the PIT in the patterned metasurface composed of the graphene ribbons and the graphene strips, which is caused by destructive interference between the superradiant mode and the subradiant mode. Interestingly, the dual-mode on-to-off modulation of PIT can be achieved by two gate voltages applied to the graphene ribbons and the graphene strips. Moreover, an absorption rate of 50% and slow-light property of 0.7 ps are achieved, demonstrating the proposed PIT metasurface has important applications in absorption and slow-light. Furthermore, coupling effects between the graphene ribbons and the graphene strips in PIT metasurface with different structural parameters are studied in detail. Thus, this work provides potential applications for the implementation of dual-mode on-to-off multifunction modulators.

Abbreviations

CMT: Coupled mode theory; CVD: Chemical vapor deposition.; FDTD: Finite-difference time-domain; MDM: Metal-dielectric-metal; PIT: Plasmon-induced transparency; SPPs: Surface plasmon polaritons

Authors' Contributions

ZML and EDG designed the study and analyzed the data. ZBZ, HJL, HX, XZ, XL, and FQZ helped in data analysis and the manuscript modification. All the authors have read and approved the final manuscript.

Funding

This work was supported by The National Natural Science Foundation of China (nos. 11847026, 61764005, and 11804093); The Scientific Project of Jiangxi Education Department of China (no. GJJ160532); The Graduate Education Reform Project of Jiangxi Province of China (no. JXYJG-2017-080); Natural Science Foundation of Jiangxi Province (no. 20192BAB212003)

Availability of Data and Materials

All data generated or analyzed during this study are included in this published article.

Competing Interests

The authors declare that they have no competing interests.

Author details

[1]School of Science, East China Jiaotong University, Nanchang 330013, China. [2]Department of Materials Science and Engineering, The Ohio State University, 2041 College Road, Columbus, OH 43210, USA. [3]School of Physics and Electronics, Central South University, Changsha 410083, China.

Received: 6 November 2019 Accepted: 23 December 2019
Published online: 02 January 2020

References

1. Barnes WL, Dereux A, Ebbesen TW (2003) Surface plasmon subwavelength optics. Nature 424:824
2. Yan S, Zhang M, Zhao X, Zhang Y, Wang J, Jin W (2017) Refractive index sensor based on a metal–insulator–metal waveguide coupled with a symmetric structure. Sensors 17:2879
3. Xu H, Li H, Li B, He Z, Chen Z, Zheng M (2016) Influential and theoretical analysis of nano-defect in the stub resonator. Sci Rep 6:30877
4. Gao E, Liu Z, Zhou F, Zhang Z (2019) Multiphase resonant properties in metallic dielectric gratings with three-slits. Mod Phys Lett B 33:1950250
5. Ren F, Chen W, Zhangsun T, Zhang Y, Fan X, Wang J (2018) Variable-Ratio Mode-Insensitive 1 × 2 Power Splitter Based on MMI Couplers and Phase Shifters. IEEE Photonics J. 10:1–12
6. Rakhshani MR, Mansouribirjandi MA (2016) Dual wavelength demultiplexer based on metal–insulator–metal plasmonic circular ring resonators. J. Mod. Opt. 63:1–9
7. Xie Y, He C, Li J, Song T, Mao Q (2016) Theoretical investigation of a plasmonic demultiplexer in MIM waveguide crossing with multiple side-coupled hexagonal resonators. IEEE Photonics J 8:4802512
8. Xiong C, Li H, Xu H, Zhao M, Zhang B, Liu C, Wu K (2019) Coupling effects in single-mode and multimode resonator-coupled system. Opt Express 27:17718–17728
9. Rahman MZU, Krishna KM, Reddy KK, Babu MV, Mirza SS, Fathima SY (2018) Ultra-wide-band band-pass filters using plasmonic MIM waveguide-based ring resonators. IEEE Photonics Tech L 30:1
10. He ZH, Zhou ZP (2018) Theoretically analyze the tunable wide band-stop filtering in plasmonic waveguide coupled with fixed height to length stubs. IEEE Photonics J. 10:1–8
11. Rakhshani MR, Mansouri-Birjandi MA (2016) High sensitivity plasmonic sensor based on metal–insulator–metal waveguide and hexagonal-ring cavity with round-corners. IEEE Sensors J. 16:3041–3046
12. He Z, Li H, Li B, Chen Z, Xu H, Zheng M (2016) Theoretical analysis of ultrahigh figure of merit sensing in plasmonic waveguides with a multimode stub. Opt Lett 41:5206
13. Chen J, Badioli M, Alonso-González P, Thongrattanasiri S, Huth F, Osmond J, Spasenović M, Centeno A, Pesquera A, Godignon P (2012) Optical nano-imaging of gate-tunable graphene plasmons. Nature 487:77
14. Grigorenko AN, Polini M, Novoselov KS (2012) Graphene plasmonics. Nat Photonics 6:749–758
15. Xu H, Zhao M, Chen Z, Zheng M, Xiong C, Zhang B, Li H (2018) Sensing analysis based on tunable Fano resonance in terahertz graphene-layered metamaterials. J Appl Phys 123:203103
16. Ruan B, You Q, Zhu J, Wu L, Guo J, Dai X, Xiang Y (2018) Fano resonance in double waveguides with graphene for ultrasensitive biosensor. Opt Express 26:16884–16892
17. Luo X, Liu Z, Cheng Z, Liu J, Lin Q, Wang L (2018) Polarization-insensitive and wide-angle broadband absorption enhancement of molybdenum disulfide in visible regime. Opt. Express 26:33918
18. Luo X, Liu ZM, Wang LL, Liu JP, Lin Q (2018) Tunable ultra-narrowband and wide-angle graphene-based perfect absorber in the optical communication region. Appl Phys Express 11:105102
19. Luo X, Cheng ZQ, Zhai X, Liu ZM, Li SQ, Liu JP, Wang LL, Lin Q, Zhou YH (2019) Nanoscale Res. Lett. 14:337
20. Chang WS, Lassiter B, Pattanawit S, Heidar S, Saumyakanti K (2012) A Plasmonic Fano Switch. Nano Lett 12:4977
21. Cao T, Wei C, Simpson RE, Zhang L, Cryan MJ (2014) Fast tuning of double Fano resonance using a phase-change metamaterial under low power intensity. Sci Rep 4:4463
22. Nasari H, Abrishamian MS, Berini P (2016) Nonlinear optics of surface plasmon polaritons in subwavelength graphene ribbon resonators. Opt Express 24:708–723
23. Xu H, Li H, He Z, Chen Z, Zheng M, Zhao M (2017) Dual tunable plasmon-induced transparency based on silicon-air grating coupled graphene structure in terahertz metamaterial. Opt. Express 25:20780–20790
24. Liu C, Li H, Xu H, Zhao M, Xiong C, Zhang B, Wu K (2019) Slow light effect based on tunable plasmon-induced transparency of monolayer black phosphorus. J Phys D Appl Phys. 52:405203
25. Zhang B, Li H, Xu H, Zhao M, Xiong C, Liu C, Wu K (2019) Absorption and slow-light analysis based on tunable plasmon-induced transparency in patterned graphene metamaterial. Opt Express 27:3598–3608
26. Gao E, Liu Z, Li H, Xu H, Zhang Z, Luo X, Xiong C, Liu C, Zhang B, Zhou F (2019) Dynamically tunable dual plasmon-induced transparency and absorption based on a single-layer patterned graphene metamaterial. Opt. Express 27:13884
27. He Z, Li H, Zhan S, Li B, Chen Z, Xu H (2015) Tunable Multi-switching in Plasmonic Waveguide with Kerr Nonlinear Resonator. Sci. Rep. 5:15837
28. Wu C, Khanikaev AB, Shvets Broadband G (2011) Slow Light Metamaterial Based on a Double-Continuum Fano Resonance. Phys. Rev. Lett. 106:107403

29. Qiu TH (2015) Electromagnetically induced holographic imaging in hybrid artificial molecule. Opt. Express 23:24537
30. Phillips DF, Fleischhauer A, Mair A, Walsworth RL, Lukin MD (2001) Storage of light in atomic vapor. Phys. Rev. Lett. 86:783
31. Lei W, Wei C, Weiwei L, Zenghong M, Chenglin D, Xinzheng Z, Jingjun X (2014) Mid-infrared plasmon induced transparency in heterogeneous graphene ribbon pairs. Opt. Express 22:32450–32456
32. Xu H, Zhao M, Zheng M, Xiong C, Zhang B, Peng Y, Li H (2019) Dual plasmon-induced transparency and slow light effect in monolayer graphene structure with rectangular defects. J. Phys. D: Appl. Phys. 52:025104
33. Zhao M, Xu H, Xiong C, Zheng M, Zhang B, Xie W, Li H (2018) Investigation of tunable plasmon-induced transparency and slow-light effect based on graphene bands. Appl. Phys. Express 11:082002
34. Xu H, Li H, Chen Z, Zheng M, Zhao M, Xiong C, Zhang B (2018) Novel tunable terahertz graphene metamaterial with an ultrahigh group index over a broad bandwidth. Appl. Phys. Express 11:042003
35. Gao E, Liu Z, Li H, Xu H, Zhang Z, Zhang X, Luo X, Zhou F (2019) Dual plasmonically induced transparency and ultra-slow light effect in m-shaped graphene-based terahertz metasurfaces. Appl Phys Express 12:126001
36. Won SJ, Alexander K, Magnuson CW, Yufeng H, Samir A, A. J, Swan AK, Goldberg BB, Ruoff RS (2011) Transfer of CVD-grown monolayer graphene onto arbitrary substrates. Acs Nano 5:6916–6924
37. He X, Zhao ZY, Shi W (2015) Graphene-supported tunable near-IR metamaterials. Opt. Lett. 40:178–181
38. Chen HT, Padilla WJ, Zide JM, Gossard AC, Taylor AJ, Averitt RD (2006) Active terahertz metamaterial devices. Nature 444:597–600
39. He X (2015) Tunable terahertz graphene metamaterials. Carbon 82:229–237
40. Cheng H, Chen S, Yu P, Duan X, Xie B, Tian J (2013) Dynamically tunable plasmonically induced transparency in periodically patterned graphene nanostrips. Appl. Phys. Lett. 103:36
41. Efetov DK, Kim P (2010) Controlling electron-phonon interactions in graphene at ultrahigh carrier densities. Phys Rev Lett 105:256805
42. Balci S, Balci O, Kakenov N, Atar FB, Kocabas C (2016) Dynamic tuning of plasmon resonance in the visible using graphene. Opt. Lett. 41:1241
43. Falkovsky LA (2008) Optical properties of graphene. J Exp Theor Phys 115: 012004
44. Falkovsky LA, Pershoguba SS (2007) Optical far-infrared properties of a graphene monolayer and multilayer. Phys Rev B 76:153410
45. Hajati Y, Zanbouri Z, Sabaeian M (2018) Low-loss and high-performance mid-infrared plasmon-phonon in graphene-hexagonal boron nitride waveguide. J Opt Soc Am B 35:446
46. Gan CH, Chu HS, Li EP (2012) Synthesis of highly confined surface plasmon modes with doped graphene sheets in the midinfrared and terahertz frequencies. Phys. Rev. B-Condens Mat. 85:117–122
47. Zou CL, Shu FJ, Sun FW, Chen WC (2014) Ultralong distance coupling between deformed circular microcavities. J Opt Soc Am B 31:478–483
48. Ju L, Geng B, Horng J, Girit C, Martin M, Hao Z, Bechtel HA, Liang X, Zettl A, Shen YR (2011) Graphene plasmonics for tunable terahertz metamaterials. Nat Nanotechnol. 6:630–634
49. Gao W, Shu J, Qiu C, Xu Q (2012) Excitation of plasmonic waves in graphene by guided-mode resonances. Acs Nano 6:7806
50. Xia SX, Zhai X, Wang LL, Lin Q, Wen SC (2016) Localized plasmonic field enhancement in shaped graphene nanoribbons Opt. Express 24:16336
51. Christensen J, Manjavacas A, Thongrattanasiri S, Koppens FHL, Abajo FJGD (2012) Graphene plasmon waveguiding and hybridization in individual and paired nanoribbons. Acs Nano 6:431–440
52. Xie F, Li HJ, Liu JP, Wang LL, Xia SX, Zhai X, Luo X, Shang XJ (2016) Graphene-based long-range SPP hybrid waveguide with ultra-long propagation length in mid-infrared range Opt. Express 24:5376–5386
53. Maier SA (2007) Plasmonics : fundamentals and applications, vol 52. Springer, Berlin, pp 49–74
54. Li HJ, Wang LL, Zhang BH, Zhai X (2016) Tunable edge-mode-based mid-infrared plasmonically induced transparency in the coupling system of coplanar graphene ribbons. Appl Phys Express 9:012001

Publisher's Note